Nitric oxide regulates K^+ and Cl^- channels in guard cells through a subset of abscisic acid-evoked signaling pathways

Carlos Garcia-Mata*†, Robert Gay†‡, Sergei Sokolovski†‡, Adrian Hills‡, Lorenzo Lamattina*, and Michael R. Blatt‡§

‡Laboratory of Plant Physiology and Biophysics, Bower Building, Institute of Biomedical and Life Sciences, University of Glasgow, Glasgow G12 8QQ, United Kingdom; and *Institutos de Investigaciones Biologicas, Universidad Nacional de Mar del Plata, 7600 Mar del Plata Buenos Aires, Argentina

Communicated by Hans Janos Kende, Michigan State University, East Lansing, MI, July 14, 2003 (received for review May 14, 2003)

Abscisic acid (ABA) triggers a complex sequence of signaling events that lead to concerted modulation of ion channels at the plasma membrane of guard cells and solute efflux to drive stomatal closure in plant leaves. Recent work has indicated that nitric oxide (NO) and its synthesis are a prerequisite for ABA signal transduction in *Arabidopsis* and *Vicia* guard cells. Its mechanism(s) of action is not well defined in guard cells and, generally, in higher plants. Here we show directly that NO selectively regulates Ca^{2+}-sensitive ion channels of *Vicia* guard cells by promoting Ca^{2+} release from intracellular stores to raise cytosolic-free $[Ca^{2+}]$. NO-sensitive Ca^{2+} release was blocked by antagonists of guanylate cyclase and cyclic ADP ribose-dependent endomembrane Ca^{2+} channels, implying an action mediated via a cGMP-dependent cascade. NO did not recapitulate ABA-evoked control of plasma membrane Ca^{2+} channels and Ca^{2+}-insensitive K^+ channels, and NO scavengers failed to block the activation of these K^+ channels evoked by ABA. These results place NO action firmly within one branch of the Ca^{2+}-signaling pathways engaged by ABA and define the boundaries of parallel signaling events in the control of guard cell movements.

cGMP-mediated signaling | stress physiology | cyclic ADP ribose | cytosolic-free $[Ca^{2+}]$ elevation | *Vicia*

The gas nitric oxide (NO) is a highly reactive free radical that serves as a cellular signaling molecule. It is a byproduct of several cellular reactions and a natural constituent of all living cells, but its functions are known principally from studies of mammalian physiology (1–3). In animals, NO acts indirectly through guanylate cyclase to activate cGMP-dependent cellular responses and directly through *S*-nitrosylation of elements downstream of several signal cascades (3). Among others, NO affects the gating of Ca^{2+}-dependent K^+ channels, Ca^{2+}, and Na^+ channels (4–6).

Evidence increasingly points to a role for NO also in plant development, stress responses, and programmed cell death (7, 8), although its situation within any one signal cascade is still poorly understood. NO action on stomatal guard cells is a case in point. Guard cells open and close the stoma of higher-plant leaves to balance gas exchange for photosynthesis against water loss via transpiration (9–11). NO enhances plant tolerance to drought (7) and contributes to stomatal closure evoked by the water-stress hormone abscisic acid (ABA). In plants, NO is produced from NO_2 through photoconversion by carotenoids, reaction with nitrate reductases (NRs) (7, 12), and with glycine decarboxylase (13). In NR-deficient *Arabidopsis*, stomata fail to close in ABA (14). Furthermore, NO scavengers suppress ABA action in closing stomata, and NO donors promote closure in the absence of ABA (15, 16). However, NR-deficient *Arabidopsis* does not show a wilty phenotype (14). Thus, although NO seems to play a role in water-stress signaling, its situation within ABA-related signaling pathways and its relationship to ion transport that drives stomatal movement has remained unclear.

ABA closes stomata by regulating guard cell membrane transport to promote osmotic solute loss. Among its actions, ABA raises cytosolic-free $[Ca^{2+}]$ ($[Ca^{2+}]_i$) and cytosolic pH (pH_i); these signals inactivate inward-rectifying K^+ channels ($I_{K,in}$) to prevent K^+ uptake and activate outward-rectifying K^+ channels ($I_{K,out}$) and Cl^- (anion) channels (I_{Cl}) at the plasma membrane to facilitate solute efflux (9, 10, 17). To explore NO function in guard cells and its association with ABA signal transduction, we recorded guard cell membrane current under voltage clamp and $[Ca^{2+}]_i$ using fura 2 fluorescence ratio imaging. Our results demonstrate that NO promotes intracellular Ca^{2+} release and thereby regulates guard cell ion channels via a subset of signaling pathways enlisted by ABA.

Materials and Methods

Plant Material and Electrophysiology. Protoplasts and epidermal strips were prepared from *Vicia faba* L., and operations were carried out on a Zeiss Axiovert microscope with ×63 long working distance differential interference contrast microscopy optics (18, 19). Patch pipettes were pulled with a Narashige (Tokyo) PP-83 puller, and currents were recorded and analyzed as described (18, 20). Voltage-clamp recordings and fura 2 injections of intact guard cells were carried out by impalement with two- and three-barrelled microelectrodes (19, 20).

$[Ca^{2+}]_i$ Measurements. $[Ca^{2+}]_i$ was determined by fura 2 fluorescence ratio imaging with a GenIV-intensified Pentamax-512 charge-coupled device camera (Princeton Instruments, Trenton, NJ) (20). Measurements were corrected for background before loading and analyzed with Universal Imaging software (Media, PA). Fura 2 fluorescence was calibrated *in vitro* and *in vivo* after permeabilization (19). Estimates of loading indicated final fura 2 concentrations $<10\ \mu M$ (19).

Numerical Analysis. Currents from intact cells were recorded and analyzed with HENRY II software (Y-Science, Glasgow, U.K., www.gla.ac.uk/ibls/BMB/mrb/lppbh.htm). Channel amplitudes were calculated from point-amplitude histograms of openings >5 ms in duration beyond closed levels, and channel number, openings, and probabilities were determined as described (18, 20). Results are reported as means ± SE.

Chemicals and Solutions. Intact cells were bathed in 5 mM Ca-Mes, pH 6.1 [Mes titrated to its pKa with $Ca(OH)_2$] with 10 mM KCl or 15 mM CsCl/15 mM tetraethylammonium-Cl to verify Cl^- currents (21). Protoplasts were bathed in Ba^{2+}-Hepes, pH 7.5

Abbreviations: ABA, abscisic acid; $[Ca^{2+}]_i$, cytosolic-free Ca^{2+} concentration; pH_i, cytosolic pH; $I_{K,in}$, inward-rectifying (Ca^{2+}-sensitive) K^+ channel (current); $I_{K,out}$, outward-rectifying (Ca^{2+}-insensitive) K^+ channel (current); I_{Cl}, Cl^- (anion) channel (current); SNAP, *S*-nitroso-*N*-acetyl-penacillamine; ODQ, 1-H-(1, 2, 4)-oxadiazole-[4,3-a]quinolxalin-1-one; SNP, sodium nitroprusside; cPTIO, 2-carboxyphenyl-4,4,5,5-tetramethylimidazoline-1-oxyl-3-oxide; cADPR, cyclic ADP ribose; CNGC, cyclic nucleotide-gated ion channel.

†C.G.-M., R.G., and S.S. contributed equally to this work.

§To whom correspondence should be addressed. E-mail: m.blatt@bio.gla.ac.uk.

www.pnas.org/cgi/doi/10.1073/pnas.1434381100

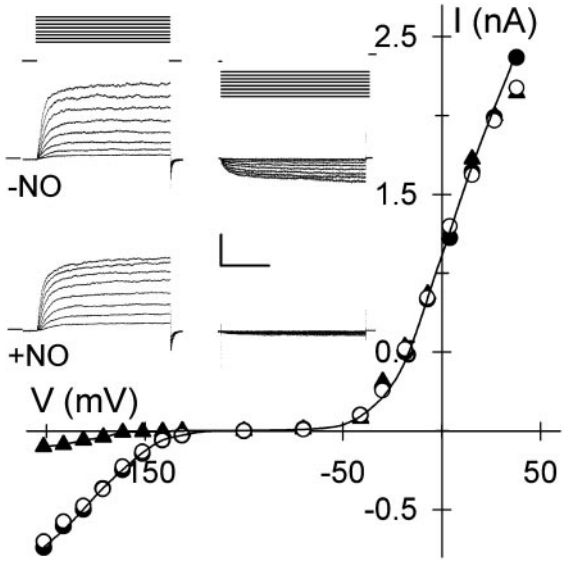

Fig. 1. NO selectively inactivates $I_{K,in}$. Voltage-clamp recordings from an intact *Vicia* guard cell are shown. (*Inset*) Steady-state current–voltage curves determined from voltage-clamp steps before (●), after 2 min of exposure to 10 μM SNAP (▲), and after 6 min of washing in buffer-SNAP (○). K^+-channel currents were obtained by subtracting instantaneous current from steady-state current at each voltage. Data for $I_{K,in}$ and $I_{K,out}$ were fitted jointly (solid lines) to common Boltzmann functions (20, 24) with the voltage sensitivity parameter $V_{1/2}$, the voltage giving half-maximal conductance, free to vary between curves. Values for $V_{1/2}$ ($I_{K,in}$): −NO, −173 ± 4 mV; +NO, −192 ± 9 mV. (*Inset*) Current traces for $I_{K,out}$ (*Left*) and $I_{K,in}$ (*Right*) before (*Middle*) and during (*Bottom*) NO treatment. Zero current is indicated on the left. Voltage protocols (*Top*) of steps between −200 and +50 mV from holding voltage of −100 mV are shown. (Scale: horizontal, 2 s; vertical, 1 nA.)

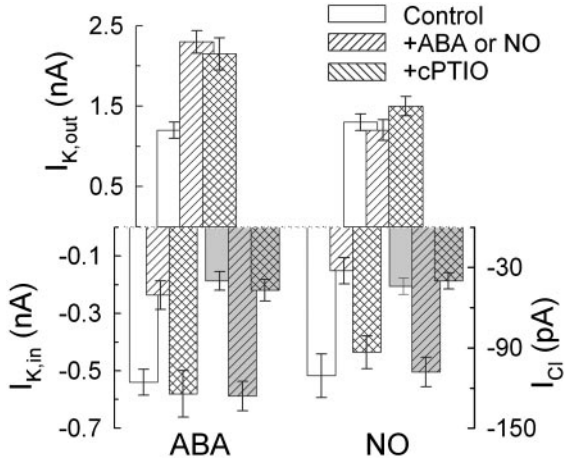

Fig. 2. NO scavenger cPTIO blocks inactivation of $I_{K,in}$ and activation of I_{Cl} by ABA and NO but not ABA-mediated activation of $I_{K,out}$. Steady-state current determined as described for Fig. 1 for $I_{K,out}$ at +30 mV, $I_{K,in}$ at −200 mV, and I_{Cl} at −70 mV (shaded bars) (21) summarizes effects of a 10-min exposure to ABA with (n = 9) or without 20 μM cPTIO (n = 8) (*Left*) and to 10 μM SNAP with (n = 7) or without 20 μM cPTIO (n = 27) (*Right*).

[Hepes buffer titrated to its pKa with $Ba(OH)_2$] adjusted to 300 milliosmolar with sorbitol, and pipettes were filled with similar solutions. For cell-attached recording, pipette and bath contained 30 mM Ba^{2+}; for whole-cell recording, pipettes contained 1 mM Ba^{2+} and $(Mg^{2+})_2ATP$, and the bath contained 30 mM Ba^{2+}; and for excised, inside-out patches, pipettes contained 30 mM Ba^{2+}, and the bath contained 1 mM Ba^{2+} and $(Mg^{2+})_2ATP$. *S*-nitroso-*N*-acetyl-penacillamine (SNAP) was dissolved in 1:1 ethanol/H_2O, and 1-H-(1,2,4)-oxadiazole-[4,3-a]quinolxalin-1-one (ODQ) was dissolved in DMSO before 1,000-fold dilution for use. Ethanol and DMSO alone at this concentration had no effect (18, 19). Sodium nitroprusside (SNP), the NO scavenger 2-carboxyphenyl-4,4,5,5-tetramethylimidazoline-1-oxyl-3-oxide (cPTIO), and all other compounds were used directly. NO generated from 10 μM SNP and SNAP was determined via metahemoglobin formation (22) to yield 10 nM/min. All reagents were from Sigma or Calbiochem.

Results

NO Targets $I_{K,in}$ and I_{Cl}. We used the membrane-permeant NO donors SNAP and SNP and the NO scavenger cPTIO while recording membrane current from intact *Vicia* guard cells under voltage clamp. Fig. 1 shows current traces and steady-state current–voltage curves from one guard cell recorded before and after a 60-s exposure to 10 μM SNAP, yielding 10 nM NO per min. Voltage steps positive of −50 mV were marked by an outward current, typical of $I_{K,out}$, that relaxed to a new steady state with half-times near 300 ms; steps negative of −120 mV gave an inward current characteristic of $I_{K,in}$. SNAP exposure dramatically reduced the amplitude of $I_{K,in}$. This response was complete within 60 s, and the effect was reversed after washing for 2 min with 20 μM cPTIO. $I_{K,out}$ was not affected by the NO donor at this concentration even after 10 min of exposure. Similar results were obtained in 27 experiments with SNAP (see Fig. 2) and with 10 μM SNP (n = 22; data not shown). $I_{K,in}$ inactivation was reversed either after adding cPTIO or after 4–6 min of washing in buffer alone. NO treatment also led to a reversible, 2.1- ± 0.4-fold increase in background current (Fig. 2) identified with I_{Cl} at the plasma membrane (21, 23), indicating a significant rise in I_{Cl} in response to NO.

We determined half-times for current activation from guard cells for which $I_{K,in}$ could be resolved in NO. Mean half-times at −200 mV were 314 ± 35 ms before treatments. After 2 min in SNAP and SNP, half-times were 538 ± 72 (n = 8) and 593 ± 85 (n = 6), respectively, indicating a substantial change in channel gating. Fitting current–voltage curves before and during NO treatments jointly to a Boltzmann function showed a change in voltage sensitivity, thus supporting this conclusion. Fittings probably underestimated the change in voltage sensitivity with NO, because data points were restricted to voltages at or greater than −200 mV. Even so, best fittings gave half-maximal activation voltages, $V_{1/2}$, displaced by ≥18 mV negative in NO (Fig. 1). Thus, similar to the effect of ABA (11), inactivation of $I_{K,in}$ by NO entailed changes in $I_{K,in}$ gating.

Because NO scavengers suppress ABA-evoked stomatal closing (15, 16), we were interested to determine whether this action, similar to that of the NO donors, was selective for $I_{K,in}$ and I_{Cl} over $I_{K,out}$. We recorded membrane currents before and after adding 10 μM ABA either in the presence or absence of 20 μM cPTIO. The results (Fig. 2) showed that the NO scavenger prevented $I_{K,in}$ inactivation and I_{Cl} activation but was without influence on the increase in $I_{K,out}$ evoked by ABA (11). These results discounted any general inhibitory effects of the NO donors or cPTIO and prompted us to examine signal cascades associated specifically with the inward-rectifying K^+ channels.

$I_{K,in}$ Inactivation and I_{Cl} Activation by NO Requires Elevated $[Ca^{2+}]_i$. Guard cell K^+ channels are known to be controlled by at least two separate signaling pathways in ABA. $I_{K,in}$ and I_{Cl} respond to increases in $[Ca^{2+}]_i$ (9–11). Effects on $I_{K,in}$ of elevating $[Ca^{2+}]_i$ include a slowing of the current kinetics and negative shift in its voltage sensitivity. $I_{K,out}$ is $[Ca^{2+}]_i$-insensitive and is regulated instead by a slower, ABA-evoked rise in pH_i (10, 11). These parallels led us to explore NO action in elevating $[Ca^{2+}]_i$.

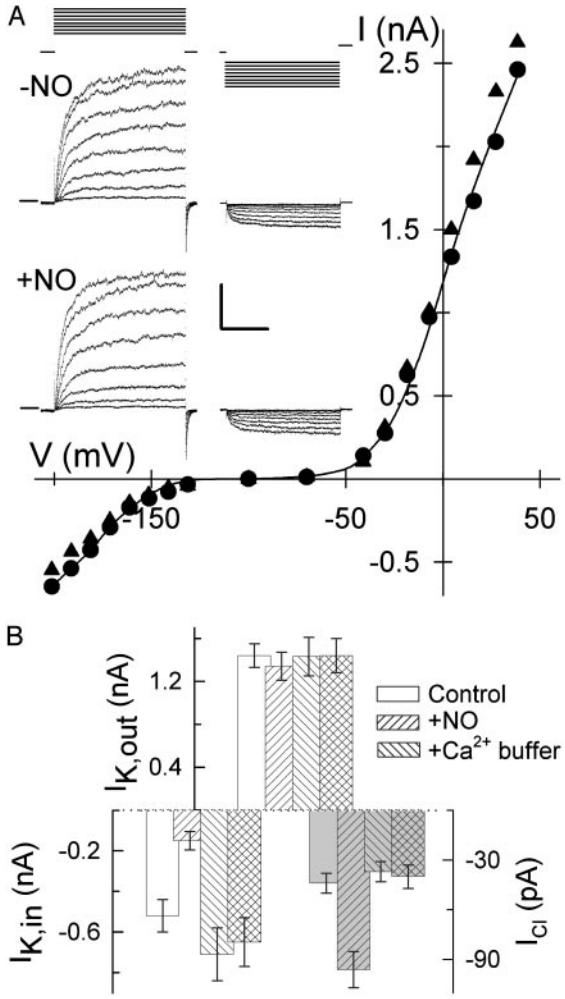

Fig. 3. Ca^{2+} buffering blocks NO inactivation of $I_{K,in}$ and activation of I_{Cl}. (*A*) Voltage-clamp recordings from an intact *Vicia* guard cell impaled and buffer-loaded from a microelectrode containing 50 mM 1,2-bis(2-aminophenoxy)ethane-*N*,*N*,*N*′,*N*′-tetraacetate (BAPTA). Shown are steady-state current–voltage curves determined from voltage-clamp steps (*Inset*) before (●) and after 6 min of exposure to 10 μM SNAP (▲) as described for Fig. 1. Data for $I_{K,in}$ and $I_{K,out}$ fitted jointly (solid lines) to common Boltzmann functions (see Fig. 1) gave half-maximal conductance for $I_{K,in}$ of -178 ± 3 mV (−NO) and -181 ± 4 mV (+NO). (*Inset*) Current traces for $I_{K,out}$ (*Left*) and $I_{K,in}$ (*Right*) before (*Middle*) and during (*Bottom*) NO treatment. Zero current is indicated on the left. Voltage protocols (*Top*) of steps between −200 mV and +50mV from holding voltage of −100 mV. (Scale: horizontal, 2 s; vertical, 1 nA.) (*B*) Summary of $I_{K,out}$, $I_{K,in}$, and I_{Cl} (shaded bars) before and after exposure to 10 μM SNAP with (n = 10) and without (n = 27) 50 mM EGTA or 50 mM BAPTA loading. Currents were determined as described for Figs. 1 and 2.

We suppressed changes in $[Ca^{2+}]_i$ by loading guard cells from microelectrodes containing Ca^{2+} buffer, either 50 mM EGTA (n = 2) or 50 mM 1,2-bis(2-aminophenoxy)ethane-*N*,*N*,*N*′,*N*′-tetraacetate (n = 8), before adding SNAP (Fig. 3). Alone, Ca^{2+} buffering led to a small but not very significant rise in $I_{K,in}$ amplitude, consistent with the low Ca^{2+} sensitivity of $I_{K,in}$ below 150 nM $[Ca^{2+}]_i$ (24). Adding NO thereafter showed that the inactivation of $I_{K,in}$ and activation of I_{Cl} were suppressed almost entirely. Thus, elevated $[Ca^{2+}]_i$ is an essential precondition to transmitting the NO signal.

NO Elevates Resting and Voltage-Evoked $[Ca^{2+}]_i$ Increases. To determine whether NO affected $[Ca^{2+}]_i$, we loaded guard cells with the Ca^{2+}-sensitive dye fura 2 to quantify $[Ca^{2+}]_i$ by fluorescence ratio imaging. Ca^{2+} channels at the *Vicia* guard cell plasma membrane activate on hyperpolarization, which leads to Ca^{2+} influx and Ca^{2+}-induced Ca^{2+} release from intracellular stores (18, 19), so resting $[Ca^{2+}]_i$ was determined with the cells clamped to −50 mV. Increases in $[Ca^{2+}]_i$ were evoked by 20-s voltage steps and 90-s voltage ramps between −50 mV and −200 mV. Fluorescence from the entire cell was used to quantify the overall $[Ca^{2+}]_i$ rise and recovery. Fluorescence from a 2-μm band around the cell periphery was used to determine the voltage threshold initiating $[Ca^{2+}]_i$ increases (19, 20).

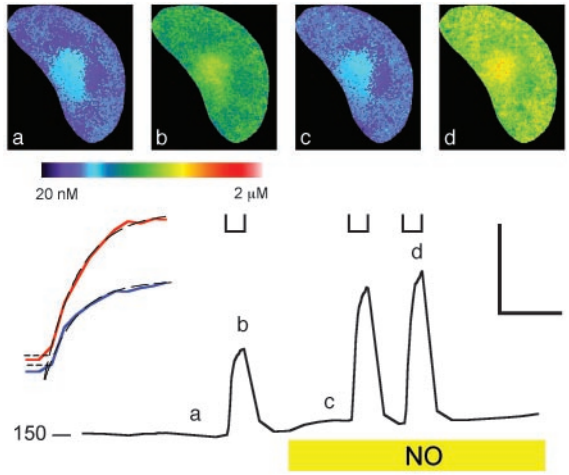

Fig. 4. NO promotes evoked $[Ca^{2+}]_i$ increases without affecting $[Ca^{2+}]_i$ recovery. (*Lower*) $[Ca^{2+}]_i$ recorded from one guard cell clamped to −50 mV and stepped to −200 mV at time periods indicated (⊔) before and after adding 10 μM SNAP show enhanced $[Ca^{2+}]_i$ rise but no apparent change in recovery kinetics at −50 mV. (*Lower Left*) $[Ca^{2+}]_i$ basal level in nM. Fura 2 fluorescence images taken at 2-s intervals. (*Upper*) Selected ratio images (*a*–*d*) correspond to the time points indicated. (*Lower Left Inset*) Expanded analysis of $[Ca^{2+}]_i$ rise from 2 s before −200 mV steps. −NO (*blue*) and +NO (*red*) show no change in lag time. The data points above +1 SD from mean $[Ca^{2+}]_i$ before clamp step (horizontal dashed lines) fitted to single exponentials gave equivalent lag periods and rise half-times of 4.2 s despite the difference in amplitudes. [Scale: horizontal, 1 min (*Lower Left Inset*, 10 s); vertical 400 nM.]

Fig. 4 shows $[Ca^{2+}]_i$ from one guard cell before and after adding SNAP. Resting $[Ca^{2+}]_i$ was close to 160 nM. Stepping the voltage to −200 mV evoked a characteristic $[Ca^{2+}]_i$ elevation to >500 nM, and $[Ca^{2+}]_i$ recovered over 1–2 min after returning to −50 mV. Maximal $[Ca^{2+}]_i$ was generally more pronounced near the perinuclear region, reflecting the high density of endoplasmic reticulum around the nucleus (see refs. 19 and 20). Adding NO led to an increase in resting $[Ca^{2+}]_i$, and after 2 min in NO, clamp steps to −200 mV evoked $[Ca^{2+}]_i$ increases to near 800 nM. Similar results were obtained in five other experiments, with NO treatment giving a significant rise in resting $[Ca^{2+}]_i$ and an enhanced response to hyperpolarizing voltage steps (Table 1). However, NO did not alter $[Ca^{2+}]_i$ recovery noticeably after voltage steps (Fig. 4).

Because Ca^{2+} must first cross the plasma membrane to trigger Ca^{2+} release and global $[Ca^{2+}]_i$ elevation, its kinetics provides a rough guide to distinguish between effects on Ca^{2+} entry and intracellular Ca^{2+} release. We fitted data recorded during steps to an exponential function to determine the rate of $[Ca^{2+}]_i$ rise within the cell and calculated the time for $[Ca^{2+}]_i$ to rise 1 SD above the mean resting $[Ca^{2+}]_i$ to estimate the delay to intracellular Ca^{2+} release. The analysis (Fig. 4 *Inset*) showed no difference in lag time to the onset of $[Ca^{2+}]_i$ increases before and after adding NO (lag times: −NO, 1.3 ± 0.1 s; +NO, 1.4 ± 0.1 s; n = 5). However, NO led to an ≈2-fold increase in the rate of

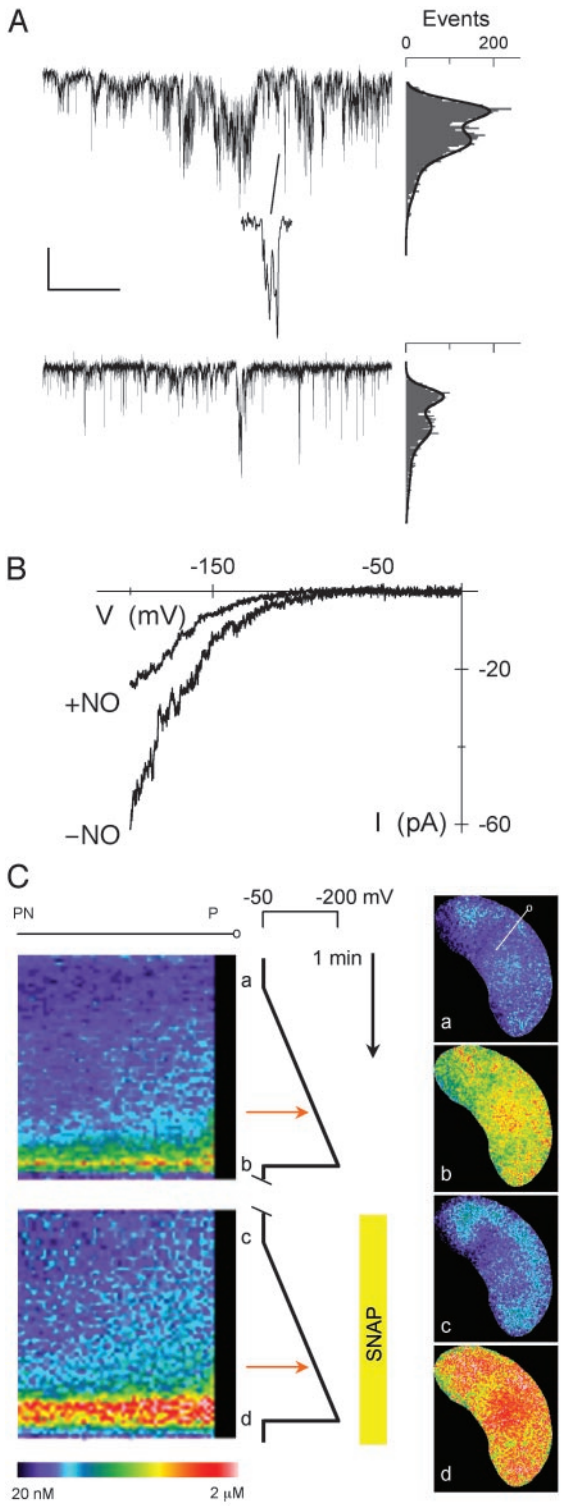

Fig. 5. NO enhances evoked $[Ca^{2+}]_i$ increases without promoting Ca^{2+}-channel activity at the plasma membrane. (*A*) Cell-attached, single Ca^{2+}-channel records from one guard cell protoplast before (*Top*) and 2 min after (*Bottom*) adding 10 μM SNAP. (*Middle*) Expanded time scale showing single opening events. [Scale: horizontal, 1 s (50 ms, *Middle*); vertical, 2 pA.] Point-amplitude histograms (*Right*), which plot the number of openings and their mean amplitude (the vertical axis is scaled to traces) for 10-s periods, including segments shown, indicate an ≈2-fold decrease in opening events. (*B*) Whole-cell Ca^{2+} currents recorded during voltage ramps before and 2 min after adding 10 μM SNAP (see ref. 18). (*C*) Kymograph (*Left*) of voltage evoked $[Ca^{2+}]_i$ rise in one intact guard cell recorded by fura 2 fluorescence ratio at 2-s intervals before and 2 min after adding 10 μM SNAP. The time line (*Center*) runs top to bottom with voltage scale and ramps as indicated. Selected ratio images (*Right*, a–d) correspond to time points indicated. The kymograph was constructed from successive ratio images averaged over a 2-pixel-wide band (line in *Right*, a) from cell exterior and periphery (P) to the perinuclear region (PN). Voltage ramps from −50 mV to −200 mV over 90 s. The threshold for $[Ca^{2+}]_i$ rise was determined as time of $[Ca^{2+}]_i$ rise 1 SD above the pre-ramp level to a depth of 3 pixel units (≈2 μm). Thresholds (red arrows, *Center*): −NO, −138 mV; +SNAP, −143 mV.

$[Ca^{2+}]_i$ rise, from 42 ± 15 nM/s before to 86 ± 16 nM/s after adding SNAP (n = 5). These results suggested a predominant effect after intracellular Ca^{2+} release rather than after Ca^{2+} entry.

NO Does Not Promote Ca^{2+}-Channel Gating at the Plasma Membrane. To assess the effect of NO on Ca^{2+} channels at the plasma membrane directly, we recorded whole-cell and single-Ca^{2+} channel currents from guard cell protoplasts. Measurements were carried out with Ba^{2+} as the charge carrier and to block K^+ channels, and Cl^- was omitted from all solutions to avoid a background of Cl^--channel activity (18, 20). In both cell-attached (Fig. 5*A*) and excised patches (data not shown), clamping to −150 mV yielded short, flickering events of 1.8 ± 0.2 pA (13 ± 1 pS, n = 6) characteristic of the Ca^{2+} channel (18, 20). No effect on single-channel conductance was observed, but adding 10 μM SNAP led to a 1.7- ± 0.5-fold reduction in the number of openings (Fig. 5*A Right*) and in single-channel activity, NP_o (−SNAP, 0.104 ± 0.004; +SNAP, 0.049 ± 0.003; n = 6). Whole-cell current recorded during voltage ramps (Fig. 5*B*) showed a 1.9- ± 0.4-fold (n = 6) decline in current that stabilized within 2 min in NO and was fully reversible after washing NO from the bath. This effect was scalar and showed no evidence of a shift in the voltage sensitivity for Ca^{2+}-channel gating that is characteristic of ABA (18).

To relate NO action on the Ca^{2+} channel with evoked $[Ca^{2+}]_i$ increases, we determined the voltage threshold for $[Ca^{2+}]_i$ rise during voltage ramps in intact guard cells. Fig. 5*C* shows data from one guard cell. Individual ratio images are shown (*Right*, a–d) corresponding to time points indicated along the voltage timeline (*Center*). The kymograph (*Left*) shows the kinetics of the $[Ca^{2+}]_i$ rise for a band stretching from the cell periphery (P) to the perinuclear (PN) region (tagged line in a, upper right). Again, a rise in resting $[Ca^{2+}]_i$ and evoked $[Ca^{2+}]_i$ increases was seen in NO. However, no difference was found in the voltage threshold evoking the $[Ca^{2+}]_i$ rise in NO (*Center*, red arrows). Indeed, on a cell-by-cell basis NO led to a reproducible negative shift in voltage evoking the $[Ca^{2+}]_i$ rise consistent with its action on the plasma membrane Ca^{2+} channels, although statistically the difference in the pooled data was not significant (−NO, −133 ± 7 mV; +NO, −145 ± 6 mV; n = 7). Thus, NO must promote $[Ca^{2+}]_i$ elevation entirely by enhancing intracellular Ca^{2+} release.

$[Ca^{2+}]_i$ Rise and $I_{K,in}$ Inactivation Are Sensitive to Antagonists of Guanylate Cyclase and Cyclic ADP Ribose (cADPR)-Mediated Ca^{2+} Release. One mechanism for $[Ca^{2+}]_i$ elevation relies on Ca^{2+} release via endomembrane Ca^{2+} channels that are activated by cADPR. In animals, cGMP stimulates cADPR biosynthesis to mobilize Ca^{2+} downstream of NO (3). Elements of one or more analogous pathways have been implicated in plant cells, including guard cells in ABA and Ca^{2+} signal processing (24, 25) and in NO (15), but their functional relationship has never been demonstrated directly.

To explore the mechanism for NO-enhanced Ca^{2+} release, we used ryanodine and ODQ, antagonists of cADPR-mediated Ca^{2+} release and of NO-sensitive guanylate cyclase, respectively, in animals that are also active in plants (15, 24, 26). Table 1

PLANT BIOLOGY

Table 1. Guanylate cyclase and cADPR antagonists suppress NO inactivation of $I_{K,in}$ and $[Ca^{2+}]_i$ elevation

Treatment	$I_{K,in}$ (pA)	$[Ca^{2+}]_i$ resting (nM)	$[Ca^{2+}]_i$ evoked (nM)
Control	−517 ± 53 (27)	159 ± 15 (6)	452 ± 31 (6)
10 μM SNAP	−151 ± 35 (27)	262 ± 31 (6)	741 ± 70 (6)
+1 μM ryanodine*	−535 ± 72 (5)	171 ± 11 (3)	200 ± 12 (3)
+20 μM ODQ	−443 ± 36 (5)	106 ± 26 (4)	303 ± 68 (4)

$I_{K,in}$ is determined as described in the Fig. 2 legend, and $[Ca^{2+}]_i$ is determined as described in the Fig. 4 legend. Data are from *n* cells.
*Partial block of evoked $[Ca^{2+}]_i$ increase reported previously (24) probably reflects the short (1-min) pretreatment used in these experiments.

summarizes $I_{K,in}$ and $[Ca^{2+}]_i$ measurements carried out as described above. Although several mechanisms for Ca^{2+} release are present in guard cells (9, 27), we found that 5-min pretreatments with ryanodine entirely suppressed $[Ca^{2+}]_i$ increases and the associated inactivation of $I_{K,in}$ (data not shown), which is consistent with the predominance of cADPR/ryanodine-sensitive Ca^{2+} release in response to voltage-evoked Ca^{2+} entry. Thereafter, NO gave no enhancement in resting $[Ca^{2+}]_i$ or evoked $[Ca^{2+}]_i$ increases, nor did it inactivate $I_{K,in}$. Pretreatment with ODQ also blocked NO action on $[Ca^{2+}]_i$ and $I_{K,in}$ but only partially suppressed evoked $[Ca^{2+}]_i$ increases and $I_{K,in}$ inactivation without NO. These results are consistent with a basal activity of ryanodine-sensitive Ca^{2+} release channels without enhanced cADPR synthesis and a requirement for NO-dependent guanylate cyclase activity and elevated cADPR levels to sensitize NO-dependent Ca^{2+} release.

Discussion

A growing body of data in recent years has linked NO to signaling in plants. Notably, genetic evidence of a prerequisite for NO synthesis in ABA-mediated stomatal control (14) has fueled debate about a link between NO, Ca^{2+}-mediated signaling, and ion-channel regulation in guard cells. Until now, however, no direct evidence has been available to delineate NO action in these or other plant cell models. Our results above unequivocally establish $[Ca^{2+}]_i$ as a principle target for NO in guard cells, demonstrating its action in promoting specifically intracellular Ca^{2+} release and, by elevating $[Ca^{2+}]_i$, in regulating Ca^{2+}-senstive K^+ and Cl^- channels at the plasma membrane. We also report that NO does not recapitulate ABA in activating plasma membrane Ca^{2+} channels and outward-rectifying (Ca^{2+}-insensitive) K^+ channels, nor does the NO scavenger cPTIO block ABA action on these K^+ channels. Thus, we unambiguously delimit the action of NO at low nanomolar concentrations to Ca^{2+} release from intracellular stores and, hence, to a subset of ABA-associated events and downstream ion-channel responses.

A key line of evidence to the targets for NO draws on the well documented separation of signals that regulate the two major K^+ channels at the guard cell plasma membrane. ABA controls $I_{K,out}$ and $I_{K,in}$ in parallel, but its action on $I_{K,in}$ depends on an early rise in $[Ca^{2+}]_i$ and only secondarily on the slower elevation in pH_i in ABA (9, 11, 24). Elevated $[Ca^{2+}]_i$ also activates I_{Cl} (ref. 10; see also Fig. 3). By contrast, $I_{K,out}$ is insensitive to $[Ca^{2+}]_i$, and its activation by ABA depends on pH_i (11). Thus, NO action clearly aligned with that of ABA-evoked changes in $[Ca^{2+}]_i$, a point we demonstrated directly in subsequent measurements of $[Ca^{2+}]_i$.

Two important downstream components of NO signaling in animals, cGMP and cADPR, function in plants and have the potential to influence $[Ca^{2+}]_i$. One mode of cGMP action in animals is to promote the biosynthesis of cADPR, which stimulates ryanodine-sensitive Ca^{2+} channels at the endoplasmic reticulum and mobilizes Ca^{2+} release (3). cADPR is known to affect Ca^{2+} release from endomembrane stores in plants including the endoplasmic reticulum (28), and in guard cells, cADPR- and ryanodine-sensitive Ca^{2+} release contribute to ABA physiology and voltage-evoked $[Ca^{2+}]_i$ increases (24, 25). A second mode of cGMP action entails binding and direct activation of cyclic nucleotide-gated ion channels (CNGCs). In animals, CNGCs are found at the plasma membrane and are active in visual, taste, and olfactory signal transduction (1, 29, 30). Less is known of plant CNGCs, but they seem to have roles in pathogen defense responses (31, 32). CNGCs have been suggested as a pathway for Ca^{2+} entry to the cytosol (15, 26), although substantive evidence is lacking. cGMP also affects Ca^{2+} sequestration through protein kinase-mediated phosphorylation that regulates Ca^{2+} ATPases (33). Finally, NO can *S*-nitrosylate the cysteines of ion channels including the cADPR/ryanodine-sensitive Ca^{2+} channel of skeletal muscle (34, 35) and epithelial K^+ channels (5, 6). Thus NO is able to regulate ion channels directly as well as affect $[Ca^{2+}]_i$ and, hence, Ca^{2+}-sensitive signaling processes via at least four different pathways for which several components are documented in plants.

Our findings point to an action of NO on Ca^{2+} release through cADPR/ryanodine-sensitive Ca^{2+} channels. Inactivation of $I_{K,in}$ and activation of I_{Cl} were blocked in guard cells preloaded with Ca^{2+} buffers (Fig. 3), discounting a significant, $[Ca^{2+}]_i$-independent action on the channels. An effect on plasma membrane Ca^{2+} channels was ruled out in single-channel and whole-cell recordings and in measurements of evoked $[Ca^{2+}]_i$ increases (Figs. 4 and 5). The same data argue against Ca^{2+} entry via NO-sensitive or rectifying (36) CNGCs or their inclusion as a significant component to the background current in NO. In plants, as in animals, most CNGCs are voltage-insensitive and nonselective (29, 31, 37), thus Ca^{2+} entry on activating these channels would depolarize the threshold for $[Ca^{2+}]_i$ elevation. By contrast, NO enhanced resting $[Ca^{2+}]_i$ and the rate and amplitude of evoked $[Ca^{2+}]_i$ rise within guard cells, although $[Ca^{2+}]_i$ recovered normally after voltage steps (Fig. 4). These results point to a sensitization of internal Ca^{2+} release but indicate that resequestration in Ca^{2+} stores was unaffected. Finally, ryanodine and ODQ, antagonists of cADPR-sensitive Ca^{2+} channels and guanylate cyclase, respectively, blocked NO action on $I_{K,in}$ and $[Ca^{2+}]_i$ (Table 1).

How might the NO signal be transmitted? In animals, a subfamily of soluble guanylate cyclases are activated by NO (3). Plant guanylate cyclases are structurally different from the animal enzymes, and an NO sensitivity has yet to be identified (38). Nonetheless, cGMP has been unambiguously demonstrated in plants by mass spectrometry (39), and an NO-sensitive guanylate cyclase is implicated in several plant tissues including *Arabidopsis* and *Vicia* guard cells, for which the physiological effects of NO are suppressed by ODQ, an inhibitor of mammalian NO-sensitive guanylate cyclase (15, 26). Thus it seems that all the major elements of an NO-driven and Ca^{2+}-coupled signal cascade occur and function in *Vicia* guard cells. We conclude that NO acts via cGMP synthesis and cADPR to sensitize endomembrane Ca^{2+} channels for Ca^{2+}-induced Ca^{2+} release.

It is clear, too, that additional transduction pathways must operate in parallel in the guard cells. A comparison with the response to ABA is instructive. In addition to enhancing $I_{K,out}$, ABA affects $[Ca^{2+}]_i$ via three separate mechanisms (18–20, 40): (*i*) similar to NO, it accelerates Ca^{2+}-induced Ca^{2+} release from intracellular stores; however, unlike NO, (*ii*) ABA alters the voltage sensitivity for gating of plasma membrane Ca^{2+} channels to promote Ca^{2+} entry across the plasma membrane, and (*iii*) it suppresses Ca^{2+} resequestration. As a consequence $[Ca^{2+}]_i$ increases in ABA, unlike NO, are triggered at membrane voltages positive of −100 mV, and once elevated, $[Ca^{2+}]_i$ recovers its previous resting level only over periods of ≥3–5 min.

Other reactive oxygen species, notably H_2O_2, have been hypothesized to play a central role in ABA signaling (41). At concentrations $\geq$50 μM, H_2O_2 affects Ca^{2+}-channel gating at the guard cell plasma membrane and elevates $[Ca^{2+}]_i$ (20, 40). However, unlike NO and ABA, exogenous H_2O_2 effects complete inactivation of both $I_{K,in}$ and $I_{K,out}$, thus eliminating a major pathway for K^+ efflux (20). By contrast, NO is permissive at low nanomolar concentrations: It engages only a subset of ABA-related events downstream that depend on elevated $[Ca^{2+}]_i$ without a significant effect on $I_{K,out}$ (Fig. 1). Only with $\geq$100 nM NO was $I_{K,out}$ seen to inactivate reversibly (data not shown), which may indicate direct *S*-nitrosylation of the K^+ channel or associated proteins (3, 42). In fact, many signaling pathways in animals originally thought to be activated by H_2O_2 actually may be controlled by other metabolites including NO (2). A requirement for NAD(P)H and reactive oxygen species in ABA signaling of guard cells (41) may be attributable at least in part to NO production by NADPH nitrate reductases (7, 14).

Finally, these findings give substance to the mechanism for stomatal closure in NO. Solute loss from the guard cells in ABA normally requires an increase in I_{Cl}, which drives the membrane positive of the K^+ equilibrium voltage (E_K) to activate $I_{K,out}$ and to balance charge for the K^+ current. K^+ uptake, in turn, is suppressed both by the voltage sensitivity of $I_{K,in}$ and through its strong inactivation by $[Ca^{2+}]_i > 200$ nM (24). In ABA, $I_{K,out}$ is enhanced by a rise in pH_i, but $I_{K,out}$ carries an appreciable current positive of E_K in the absence of ABA (Fig. 1). Thus, even at the elevated resting $[Ca^{2+}]_i$ in NO (Fig. 4 and Table 1), $I_{K,in}$ will be suppressed. Thus, together with activation of I_{Cl} (Fig. 2), NO may be expected to favor solute loss and stomatal closure, albeit at a reduced rate compared with ABA (see Fig. 1 and ref. 15).

In conclusion, we show that NO selectively regulates the Ca^{2+}-sensitive K^+ and Cl^- channels of *Vicia* guard cells by promoting Ca^{2+} release from intracellular stores to raise $[Ca^{2+}]_i$. Additional evidence points to NO action mediated by a cGMP-dependent cascade. Unlike ABA, low nanomolar concentrations of NO do not affect plasma membrane Ca^{2+} channels and Ca^{2+}-insensitive K^+ channels, nor does NO scavenging prevent ABA from activating these K^+ channels. These results place NO action firmly within a subset of the signaling pathways enlisted by ABA.

We thank Anna Amtmann for comments on the manuscript. This work was supported by Biotechnology and Biological Sciences Research Council Grants P09640, C10234, and P09561 to M.R.B., Agencia Nacional de Promoción de Ciencia y Tecnología, and a Foundation Antorchas travel grant to L.L. and C.G.-M.

1. Gibson, A. D. & Garbers, D. L. (2000) *Annu. Rev. Neurosci.* **23,** 417–439.
2. Stamler, J. S. (1994) *Cell* **78,** 931–936.
3. Ahern, G. P., Klyachko, V. A. & Jackson, M. B. (2002) *Trends Neurosci.* **25,** 510–517.
4. Renganathan, M., Cummins, T. R. & Waxman, S. G. (2002) *J. Neurophysiol.* **87,** 761–775.
5. Tang, X. D., Daggett, H., Hanner, M., Garcia, M. L., Mcmanus, O. B., Brot, N., Weissbach, H., Heinemann, S. H. & Hoshi, T. (2001) *J. Gen. Physiol.* **117,** 253–273.
6. Bolotina, V. M., Najibi, S., Palacino, J. J., Pagano, P. J. & Cohen, R. A. (1994) *Nature* **368,** 850–853.
7. Garcia-Mata, C. & Lamattina, L. (2003) *Trends Plant Sci.* **8,** 20–26.
8. Delledonne, M., Xia, Y. J., Dixon, R. A. & Lamb, C. (1998) *Nature* **394,** 585–588.
9. Hetherington, A. M. (2001) *Cell* **107,** 711–714.
10. Schroeder, J. I., Allen, G. J., Hugouvieux, V., Kwak, J. M. & Waner, D. (2001) *Annu. Rev. Plant Physiol. Plant Mol. Biol.* **52,** 627–658.
11. Blatt, M. R. (2000) *Annu. Rev. Cell Dev. Biol.* **16,** 221–241.
12. Rockel, P., Strube, F., Rockel, A., Wildt, J. & Kaiser, W. M. (2002) *J. Exp. Bot.* **53,** 103–110.
13. Chandok, M. R., Ytterberg, A. J., van Wijk, K. J. & Klessig, D. F. (2003) *Cell* **113,** 469–482.
14. Desikan, R., Griffiths, R., Hancock, J. & Neill, S. (2002) *Proc. Natl. Acad. Sci. USA* **99,** 16314–16318.
15. Neill, S. J., Desikan, R., Clarke, A. & Hancock, J. T. (2002) *Plant Physiol.* **128,** 13–16.
16. Garcia-Mata, C. & Lamattina, L. (2002) *Plant Physiol.* **128,** 790–792.
17. Blatt, M. R. (2000) *Curr. Opin. Plant Biol.* **3,** 196–204.
18. Hamilton, D. W. A., Hills, A., Kohler, B. & Blatt, M. R. (2000) *Proc. Natl. Acad. Sci. USA* **97,** 4967–4972.
19. Grabov, A. & Blatt, M. R. (1998) *Proc. Natl. Acad. Sci. USA* **95,** 4778–4783.
20. Köhler, B. & Blatt, M. R. (2002) *Plant J.* **32,** 185–194.
21. Grabov, A., Leung, J., Giraudat, J. & Blatt, M. R. (1997) *Plant J.* **12,** 203–213.
22. Murphy, M. E. & Noack, E. (1994) *Methods Enzymol.* **233,** 240–250.
23. Pei, Z. M., Kuchitsu, K., Ward, J. M., Schwarz, M. & Schroeder, J. I. (1997) *Plant Cell* **9,** 409–423.
24. Grabov, A. & Blatt, M. R. (1999) *Plant Physiol.* **119,** 277–287.
25. Leckie, C. P., McAinsh, M. R., Allen, G. J., Sanders, D. & Hetherington, A. M. (1998) *Proc. Natl. Acad. Sci. USA* **95,** 15837–15842.
26. Durner, J., Wendehenne, D. & Klessig, D. F. (1998) *Proc. Natl. Acad. Sci. USA* **95,** 10328–10333.
27. Sanders, D., Pelloux, J., Brownlee, C. & Harper, J. F. (2002) *Plant Cell* **14,** S401–S417.
28. Navazio, L., Mariani, P. & Sanders, D. (2001) *Plant Physiol.* **125,** 2129–2138.
29. Finn, J. T., Grunwald, M. E. & Yau, K. W. (1996) *Annu. Rev. Physiol.* **58,** 395–426.
30. Zagotta, W. N. & Siegelbaum, S. A. (1996) *Annu. Rev. Neurosci.* **19,** 235–263.
31. Balague, C., Lin, B. Q., Alcon, C., Flottes, G., Malmstrom, S., Kohler, C., Neuhaus, G., Pelletier, G., Gaymard, F. & Roby, D. (2003) *Plant Cell* **15,** 365–379.
32. Clough, S. J., Fengler, K. A., Yu, I. C., Lippok, B., Smith, R. K. & Bent, A. F. (2000) *Proc. Natl. Acad. Sci. USA* **97,** 9323–9328.
33. Chen, J., Wang, Y. P., Wang, Y., Nakajima, T., Iwasawa, K., Hikiji, H., Sunamoto, M., Choi, D. K., Yoshida, Y., Sakaki, Y., *et al.* (2000) *J. Biol. Chem.* **275,** 28739–28749.
34. Eu, J. P., Sun, J. H., Xu, L., Stamler, J. S. & Meissner, G. (2000) *Cell* **102,** 499–509.
35. Xu, L., Eu, J. P., Meissner, G. & Stamler, J. S. (1998) *Science* **279,** 234–237.
36. Leng, Q., Mercier, R. W., Hua, B. G., Fromm, H. & Berkowitz, G. A. (2002) *Plant Physiol.* **128,** 400–410.
37. Leng, Q., Mercier, R. W., Yao, W. Z. & Berkowitz, G. A. (1999) *Plant Physiol.* **121,** 753–761.
38. Ludidi, N. & Gehring, C. (2003) *J. Biol. Chem.* **278,** 6490–6494.
39. Brown, E. G. & Newton, R. P. (1992) *Phytochem. Anal.* **3,** 1–13.
40. Pei, Z. M., Murata, Y., Benning, G., Thomine, S., Klusener, B., Allen, G. J., Grill, E. & Schroeder, J. I. (2000) *Nature* **406,** 731–734.
41. Murata, Y., Pei, Z. M., Mori, I. C. & Schroeder, J. (2001) *Plant Cell* **13,** 2513–2523.
42. Stamler, J. S. & Meissner, G. (2001) *Physiol. Rev.* **81,** 209–237.